Influence of source images spatial characteristics on the global quality of fused images

Influencia de las características espaciales de las imágenes fuente en la calidad global de las imágenes fusionadas

C. Gonzalo[1] y M. Lillo[2]
chelo@fi.upm.es

[1]Universidad Politécnica de Madrid, Facultad de Informática, DATSI, España.
[2]Universidad de Concepción, Facultad de Ingeniería Agrícola. Departamento de Mecanización y Energía, Chile.

Recibido el 3 de Julio de 2008 , aceptado el 20 de Octubre de 2008

RESUMEN

La mayoría de las técnicas de fusión de imágenes actualmente disponibles, están basadas en análisis multirresolución. Este tipo de técnicas requieren la descomposición de las imágenes a diferentes escalas o niveles, dependiendo los resultados de fusión de dichos niveles. Es por ello, que en este trabajo se ha planteado un doble objetivo. Por un lado, investigar como influyen las características espaciales de las imágenes fuente en el nivel de descomposición en el que se debe realizar el proceso de fusión; y por otro lado, mostrar la relación existente entre el nivel de descomposición al que se someten las imágenes fuente a fusionar, con la calidad espacial-espectral de las imágenes fusionadas. Este estudio se ha llevado a cabo para un método de fusión en particular, basado en la Transformada Wavelet, calculada mediante el algoritmo à trous. La calidad de las imágenes fusionadas se ha evaluado mediante los índices ERGAS (espacial y espectral), la correlación espacial (índice de Zhou), la correlación espectral y un índice global (Q4). La metodología se ha aplicado a imágenes multiespectrales y pancromáticas registradas por los correspondientes sensores a bordo de los satélites Landsat, Ikonos, and Quickbird. Los resultados obtenidos han mostrado que, en la mayoría de los casos, se pueden obtener imágenes fusionadas de buena calidad espacial y espectral, simultáneamente, con un número pequeño de niveles de descomposición. Además,

ABSTRACT

The majority of the currently available techniques to perform remote sensed image fusion are based on multiresolution analysis. This kind of images analysis requires the decomposition of the image at differente scales or levels, depending the fusion results on this level. Then, the two main objectives of this work are: to investigate the influence of the source images spatial characteristics on the decomposition level that the process fusion should be performed in; and to show how depends the spatial-spectral quality of fused images on this decomposition level. To carry out this study, the image fusion methodology that has been applied is based on the Wavelet transform, calculated by the à trous algorithm. The quality of the fused images has been evaluated by the ERGAS indices, as well as, the spectral correlation, the spatial correlation (Zhou's index) and a global index (Q4). This methodology has been applied to fuse several multispectral and panchromatic images registered by the corresponding sensors on board the Landsat, Ikonos, and Quickbird satellites. It has been demonstrated that, in the majority of the cases, a low number of decompositions provides fused images with a high spatial and spectral quality trade-off. Additionally, the results indicate that the decomposition level that provides the best spatial-spectral quality trade-off depends on the

los resultados han mostrado que el nivel de descomposición que proporciona imágenes fusionadas con el mejor compromiso entre la calidad espacial y espectral está relacionado con el contenido de frecuencias espaciales de las imágenes fuente.

PALABRAS CLAVE: Fusión de Imágenes, índices ERGAS, Imágenes Multiespectrales, Wavelet à trous, Nivel de descomposición, Frecuencias Espaciales.

spatial frequencies content of the source images.

KEYWORDS: Images fusion, ERGAS Index, Multispectral Image, Wavelet à trous, Decomposition Level, Spatial Frequencies

INTRODUCTION

One of the principal objectives of remote sensing systems for earth observation, is data registering for determined areas of terrestrial coverage, which are useful for facilitating analysis and management at different scales: local, regional, and global; and at different times. The precision of the results provided by remote sensing techniques depends on a series of factors, among which the most notable are the sensor technology used, and consequently the characteristics of the images registered by them (spatial, spectral and temporal resolution) (Sawaya *et al*. 2003). Actually, and due to the limitations of the information transmission technology from spatial platforms, a compromise between these three resolution types exists in such a way that those sensors that provide a high spatial resolution tend to present lower spectral resolution and vice versa (Mather 1999). However, there is a wide range of remote sensing applications which require satellite images that combine high spatial and spectral resolution. The currently available images fusion techniques can improve the quality of the information registered by remote sensors, integrating the high spatial information provided by its panchromatic sensor with the spectral resolution corresponding to multispectral sensor. But, it should be noted that the spatial and spectral quality trade-off of the fused images is somewhat inherent in the fusion methods. Consequently, an improvement in the spatial quality of an image obtained from a fusion strategy implies a diminishing of the spectral quality and vice versa. In this sense, it is desirable to have fusion techniques that would objectively establish the best trade-off between spatial and spectral quality of the fused images.

The majority of the currently available techniques to perform remote sensed images fusion are based on multiresolution analysis (Mallat 1999; Ranchin *et al*. 2003; Pohl 1997; Pohl et al. 1998; Zhou et al. 1998). Being one of the most widely used the Discrete Wavelet Transform (DWT) (Mallat 1999). DWT is a linear transformation that is highly useful in the area of signal processing, where one of its principal applications consists in separating data sets into distinct frequency components, which are then represented on common scales. There are different forms of calculating the DWT to be used in fusion algorithms. One is the pyramidal algorithm of Mallat, commonly used due to the high spectral quality of resulting images; although its low anisotropic characteristic and its decimated character present some problems at the image fusion like the "saw-teeth" effect that noticeably damages the spatial quality of the fused images with a high content of borders that are not horizontal, vertical or diagonal (Candes *et al*. 2000).

An alternative algorithm, the Wavelet-à trous algorithm was proposed in (Dutilleux 1987). This algorithm presents two main differences against the pyramidal ones. First, the isotropic nature of the à trous algorithm reduces noteworthy the "saw-teeth" effect and second, it is redundant, which implies that between two consecutive decomposition levels, there is no dyadic spatial compression of the original image. That has been showed at Figure 1. In Figure 1 (a), the basis of the pyramid represents the original image and each of its levels is a decomposed, compressed version of the image represented at the previous level. In this way, spatial resolution and image size decrease from one level to the next one. However, in the Figure 1 (b), the spatial resolution decreases from one level to the next one, but not the image size, which is constant for all levels. Several works, have showed that redundant Wavelet transforms provide better results in determined image processing applications such as noise elimination (Malfait *et al*. 1997), texture classification (User 1995), and more recently in the case of image fusion (Nuñez *et al*. 1999; Chibani et al. 2003).

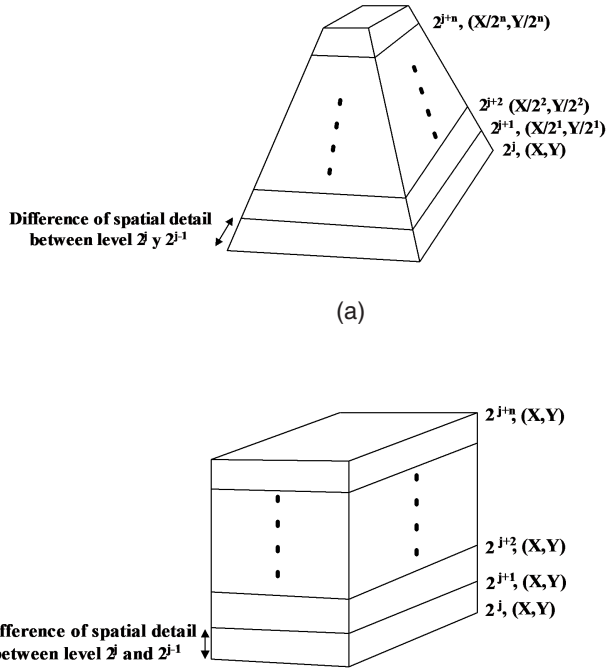

Figure 1. Decomposition outline for: (a) Mallat Algorithm, (b) à trous algorithm

Independent of the algorithm used to calculate the DWT, the images fusion techniques based on this transformation imply the determination of the number of wavelet coefficients, obtained through a decomposition process of the panchromatic image (PAN), that should be integrated in the n^{th} decomposition level of the multispectral image (MULTI), in order to obtain fused images with high and balanced spatial and spectral quality. Investigating the influence of the MULTI decomposition level (n), as well as the number of PAN Wavelet coefficients in the global quality of fused images, five different fusion schemes have been proposed and analyzed in (Gonzalo *et al.* 2004). The results obtained in the cited study have shown that when both source images are decomposed the same number of levels, the fused images present a large equilibrium between spatial and spectral quality. That means the number of PAN wavelet coefficients used should be equal to the number of times that MULTI has been decomposed.

Beginning with this idea, the question that remains to be answered is how many times the source images must be degraded in order to optimize the fusion process result, achieving images with high spatial and spectral quality and maintaining, at the same time, the best compromise between them. In this sense, one of the objectives of this work is to investigate the dependence of the spatial/spectral quality of the fused images, using the à trous algorithm (Lillo-Saavedra *et al*. 2006), with respect to the decomposition level of the source images, as well as determining the most adequate decomposition level for different types of images. A crucial point in this study is the availability of metrics that allows the estimation of the spatial/spectral quality of the fused images.

Image quality assessment plays an important role in most image processing applications. But it is especially critical in the case of image fusion, since a reference image is unavailable. On the other hand, quality evaluation of fused remote sensed images presents additional difficulties, since this kind of data exhibit spectral and spatial characteristics simultaneously, as it has been mentioned before. Therefore these two characteristics should be evaluated

in order to determine the global quality of fused remote sensed images. However, most of the developed assessment techniques are of general application (Xydeas *et al*. 2000;Qu *et al*. 2002; Piella *et al*. 2003) and they do not consider these particular objectives. In this sense, (Wald 2002) was the first author that presented an index, named ERGAS, for assessment the quality of the remote sensing fusion product. Next, a quantitative method to evaluate the spatial quality of a merged image was proposed in (Zhou *et al.* 1998), where the correlation coefficient between the high-pass filtered components of the fused and high-resolution panchromatic images was used as a quality index. It is also usual to evaluate the spectral correlation between the fused image and the original multiespectral image (Zhang *et al*. 2005). The main problem of using metrics based on correlation operations is the saturation effect. That is, large differences in the fused image characteristics do not correspond always with large differences in the metric values. In (Alparone 2004), it has been proposed a global quality measurement of pan-sharpened multispectral imagery, based in a universal image quality index previously defined by (Wang *et al*. 2002), by using the quaternion theory; however, it presents the handicap that only can be applied to four spectral bands. The ERGAS index proposed by Wald does not present saturation effects and its definition is independent of the spectral bands number. A spatial index inspired in the original ERGAS was proposed in (Lillo-Saavedra *et al.* 2005). In this sense, in this paper they will be named as spectral ERGAS and spatial ERGAS respectively. The availability of two indices that measure the spatial and spectral quality of the fused images independently, but within the same domain, allows defining global quality measures of the fused remote sensed images, such as the average ERGAS or the standard deviation, as well as, establishing a trade-off between the two characteristics. For that reason the spatial and spectral ERGAS indices have been considered in this work.

As it has been already mentioned, the fusion methodology investigated in this paper is based on the DWT computed by the à trous algorithm, in this sense, this algorithm has been described in Section 2. In Section 3, the proposed methodology to determine the decomposition level of the source images has been presented. In Section 4, data used in this paper have been described. Results and their Conclusions are included in Section 5 and 6 respectively.

OUTLINE OF THE WAVELET-À TROUS ALGORITHM

The wavelet-à trous algorithm consists basically in the application of consecutive convolutions between the image under analysis and a scaling function at distinct decomposition levels (Gónzalez-Audicana 2005; Lillo-Saavedra *et al*. 2006). One of the most widely used scaling functions for the computation of the à trous algorithm is the b3-spline (Nuñez *et al* 1999).

If the original image (without decomposition) is represented by $I_j(x,y)$, the wavelet coefficient, $C_{j+n}(x,y)$ for the decomposition level j+n, is obtained by the difference between the corresponding two consecutive degraded images, $I_{j+n-1}(x,y)$ and $I_{j+n}(x,y)$, as it is shown in equation (1):

$$C_{j+n}(x,y) = I_{j+n-1}(x,y) - I_{j+n}(x,y) \qquad (1)$$

To carry out image synthesis, from a decomposition level j+n, an additive operation should be applied in which all the coefficients obtained are added to the last decomposition level of the original image, as it is represented in equation (2).

$$I_j(x,y) = I_{j+n}(x,y) + \sum_{k=1}^{n} C_{j+k}(x,y) \qquad (2)$$

If $I_{j+n}(x,y)$ represents the last degraded plane that contains the low frequency information of the original image, and the total wavelet $\sum_{k=1}^{n} C_{j+k}(x,y)$ coefficients, which contains the high frequency information, then it is possible to plant an images fusion scheme in which the low frequency information contained in Ij+n(x,y), is added to the high frequency information contained in the wavelet coefficients of the PAN image, to obtain as result, a multispectral image with high spatial resolution.

METHODOLOGY

A formal representation of the fusion method used in this work is given by equation (3) (Nuñez *et al* 1999):

$$FUS_i(x,y) = MULTI_i^n(x,y) + \sum_{k=1}^{n} C_k^{PAN}(x,y) \quad (3)$$

Where the index i represents the spectral band of the MULTI and fused (FUS) images; n the decomposition level of source images; and $C_k^{PAN}(x,$ are the wavelet coefficients of the PAN image for the k decomposition level.

The study of the influence of the decomposition level (n) on the spatial/spectral quality of the fused images requires the measure of both qualities. In this work, the indices used were the original ERGAS (Erreur Relative Globale Adimensionalle de Synthèse) (Wald 2002), defined as:

$$ERGAS_{spectral} = 100\frac{h}{l}\sqrt{\frac{1}{N_{Bands}}\sum_{i=1}^{N_{Bands}}\left(\frac{(RMSE_{spectral}(Band_i))^2}{(\overline{MULTI_i})^2}\right)} \quad (4)$$

Where h and l represent the spatial resolution of the FUS and MULTI images, respectively; NBands is the number of bands of the fused image $\overline{MULTI_i}$ is the mean radiance value of the ith band of the MULTI image and $RMSE_{spectral}$ is defined as (5):

$$RMSE_{spectral}(Band_i) = \frac{1}{NP}\sqrt{\sum_{k=1}^{NP}(MULTI_i(k) - FUS_i(k))^2} \quad (5)$$

Where NP is the number of pixels of the fused image and FUS_i represents the i^{th} band of the fused image. Lillo-Saavedra *et al*. (2005) proposed the spatial ERGAS, defining it as in the next equation:

$$ERGAS_{spatial} = 100\frac{h}{l}\sqrt{\frac{1}{N_{Bands}}\sum_{i=1}^{N_{Bands}}\left(\frac{(RMSE_{spatial}(Band_i))^2}{(PAN_i)^2}\right)} \quad (6)$$

Where PAN_i is the image obtained by adjusting the histogram of the original PAN image to the histogram of the ith band of the fused image. $RMS_{Espatial}$ has been defined as:

$$RMSE_{spatial}(Band_i) = \frac{1}{NP}\sqrt{\sum_{k=1}^{NP}(PAN_i(k) - FUS_i(k))^2} \quad (7)$$

The comparison of equations (4) and (6) indicates that both indexes have a common variation domain. The ideal value of zero would correspond to maximum quality, and experimentally it has been demonstrated that a value less than 3 corresponds to a good quality (Wald 2002). A scheme of the protocol described above is illustrated at Fig. 2.

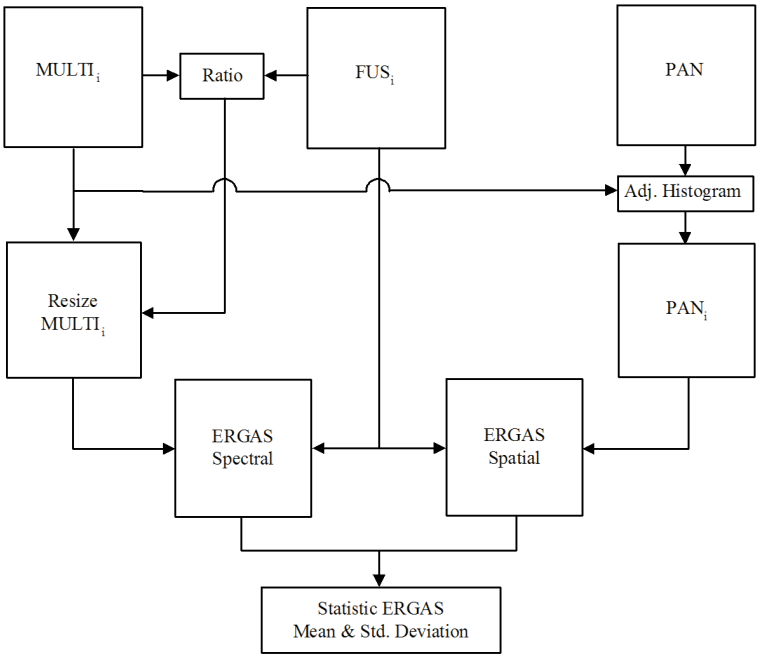

Figure 2. Protocol for computing ERGAS indices: spatial, spectral, average and standard deviation

The ERGAS indices, both spatial and spectral of several fused images, as well as their average values and standard deviations, have been evaluated and represented in a common domain, against the decomposition level (n). In all cases, it has been observed that for n>10 the sensitivity of the ERGAS decreases noteworthy. Then, it seems that it is not necessary to degrade a high number of times the source images to obtain fused images with a good quality. In fact, it has been observed, in all studied cases, that it should not be decomposed more than 5 times, in order to preserve the spectral characteristics of the original multiespectral image. In Fig. 3, the results obtained for a particular scene have been shown. It can be observed that while the decomposition level (n) increases, the spectral quality of the fused images decreases and, at the same time, their spatial quality increases. Since these results show the inherent trade-off between spatial and spectral qualities of fused images, they prove, in an empirical way, the spatial and spectral characteristics attributed to the ERGAS indices.

The value of n that establishes the best trade-off between the spatial and spectral quality can be provided by next expression:

$$ERGAS_{spectral}(n) \approx ERGAS_{spatial}(n) \qquad (8)$$

However, as a consequence of the discrete nature of the n values, it will not be always possible to find an integer value of n that satisfies the equation (8). Consequently, in this paper it is proposed as the best solution, the n value that minimizes the quality indicator defined as the multiplication of the ERGAS averages by their standard deviations.

In order to confirm the obtained results, it has been considered necessary to evaluate the fused images quality by other quality indices. The spectral quality of the fused images has been evaluated by the spectral correlation index (Zhang *et al*. 2005), defined as:

$$SC = \frac{1}{N_{bands}} \sum_{i=1}^{Nbands} Corr_i(MULTI_i, FUS_i) \qquad (9)$$

And the spatial quality has been evaluated by the Zhou's index (Zhou *et al*. 1998):

$$I_Z = \frac{1}{N_{Bands}} \sum_{i=1}^{N_{Bands}} Corr_i(PAN^{high\_pass}, FUS_i^{high\_pass}) \qquad (10)$$

where PAN^{high_pass} and $FUS_i^{high\_pass}$ represent a high-pass PAN filtered image and each one of the high pass fused filtered band, respectively. The high pass filter process, proposed by Zhou, consists in a convolution product between the image to be filtered and the Laplacian Kernel (LK), illustrated in equation (11):

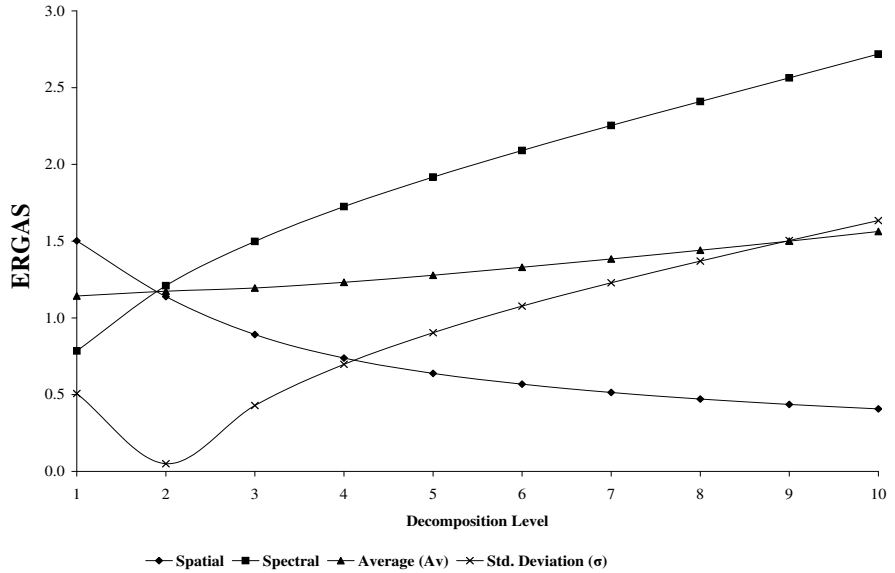

Figure 3. ERGAS indices variation respect to the decomposition level (n)

$$LK = \begin{bmatrix} -1 & -1 & -1 \\ -1 & 8 & -1 \\ -1 & -1 & -1 \end{bmatrix} \qquad (11)$$

And finally, the index Q4 (Alparone *et al*. 2004), defined in equation (12), has been used for obtaining a global measure of the quality of the fused image.

$$Q4 = \frac{4\left|\sigma_{z_1 z_2}\right| \cdot \left|\overline{Z_1}\right| \cdot \left|\overline{Z_2}\right|}{\left(\sigma_{z_1}^2 + \sigma_{z_2}^2\right)\left(\left|\overline{Z_1}\right|^2 + \left|\overline{Z_2}\right|^2\right)} \qquad (12)$$

In which, $\overline{Z_1}$ and $\overline{Z_2}$ represent the original multiespectral image and the fused image, expressed as quaternions; $\sigma_{z_1 z_2}$ denotes the hypercomplex covariance between Z_1 and $\overline{Z_2}$ and σ_{z_1} and σ_{z_2} are their hypercomplex variances.

DATA DESCRIPTION

The study presented was performed with twelve scenes with different spectral and spatial content and registered by different sensors. Four of them correspond to an image registered on 20th August, 1999 by the panchromatic and multispectral (ETM+) sensors, on board the Landsat 7 satellite. This scene is located around the city of Madrid, Spain. Other four scenes were registered, by the panchromatic and multispectral sensors of Ikonos satellite, on March 10, 2000. Geographically, they are located in the Maipo Valley, near Santiago, Chile. And the last four scenes have been extracted from an image registered on August 22, 2002 by the panchromatic and multispectral sensors of Quickbird satellite. In this case, the geographic area corresponds to the northwest area outside of Madrid, Spain.

Fig. 4 (a), (b), (c), and (d) include the NGB (Near-Green-Blue) compositions of the Landsat multiespectral scenes (L1, L2, L3 and L4), Fig. 4 (i), (j), (k) and (l) contain the NGB composition of the Ikonos multispectral scenes (IK1, IK2, IK3, IK4) and Fig. 4 (q), (r), (s), and (t); include the NGB composition of the Quickbird multiespectral scenes (QU1, QU2, QU3, QU4). The size of MULTI Landsat, Ikonos and Quickbird images scenes was 256x256, 128x128 and 512x512, respectively.

With the aim to analyze and compare the spatial frequencies content of the 12 scenes, Fast Fourier Transforms (FFT) of their panchromatic images were performed. Fig. 5 (a), (b), (c), (d), (i), (j), (k), (l), (q), (r), (s) and (t) display the panchromatic images. The representation in logarithmic scale of the FFT modules are included in Figures 5 (e), (f), (g), (h), (m), (n), (o), (p), (u), (v), (w) and (x).

The scene L1 (Figures 4 (a) and 5 (a)) corresponds to a mountainous zone, where the predominant land cover is bare soil and consequently it is characterized by a low spatial variability, as can be appreciated in Fig. 5 (e). In contrast, L2 (Fig. 4 (b) and 5 (b)) corresponds to a zone with different types of crops and some objects with strong edges, as the river in the upper left corner. Thus its FFT (Fig. 5(f)) displays higher spatial frequencies than L1. Scene L3 (Fig. 4 (c) and 5 (c)) corresponds to an urban area. The most relevant features that can be observed in it are communication ways, which provide higher spatial frequencies than for the others scenes. Scene L4 (Figures 4 (d) and 5 (d)) contains different coverage types (water, soil, paths …). The high spatial frequencies present in its Fourier Transform (Figure 5 (h)) can be due to the large amount of paths.

In the case of the Ikonos images, the scene IK1 (Figures 4 (i) and 5 (i)) corresponds to a mountainous zone characterized by a large surface area of bare soil with little plant coverage, similar to L1. Consequently, as for L1, its FFT has a low content of high spatial frequencies (Figure 5 (m)). In contrast, IK2 (Figures 4 (j) and 5 (j)) corresponds to a zone of different types of crops with a very regular plant distribution and with a small distance between rows, in each one of the plots. In other words, it has higher spatial frequency content than the other Ikonos scenes. This fact, as well as symmetries present in it can be appreciated in the FFT presented in Figure 5 (n). Notable differences can be appreciated when the FFTs of IK1 and IK2 are compared. Scene IK3 (Figure 4 (k) and 5 (k)) corresponds fundamentally to an urban area with a high number of constructions. Like IK2, it presents high regularity in object distribution; however, it is important to note that the spatial periodicity is greater and then the spatial frequency content is less, resulting in substantially different FFTs (Figure 5 (o)).

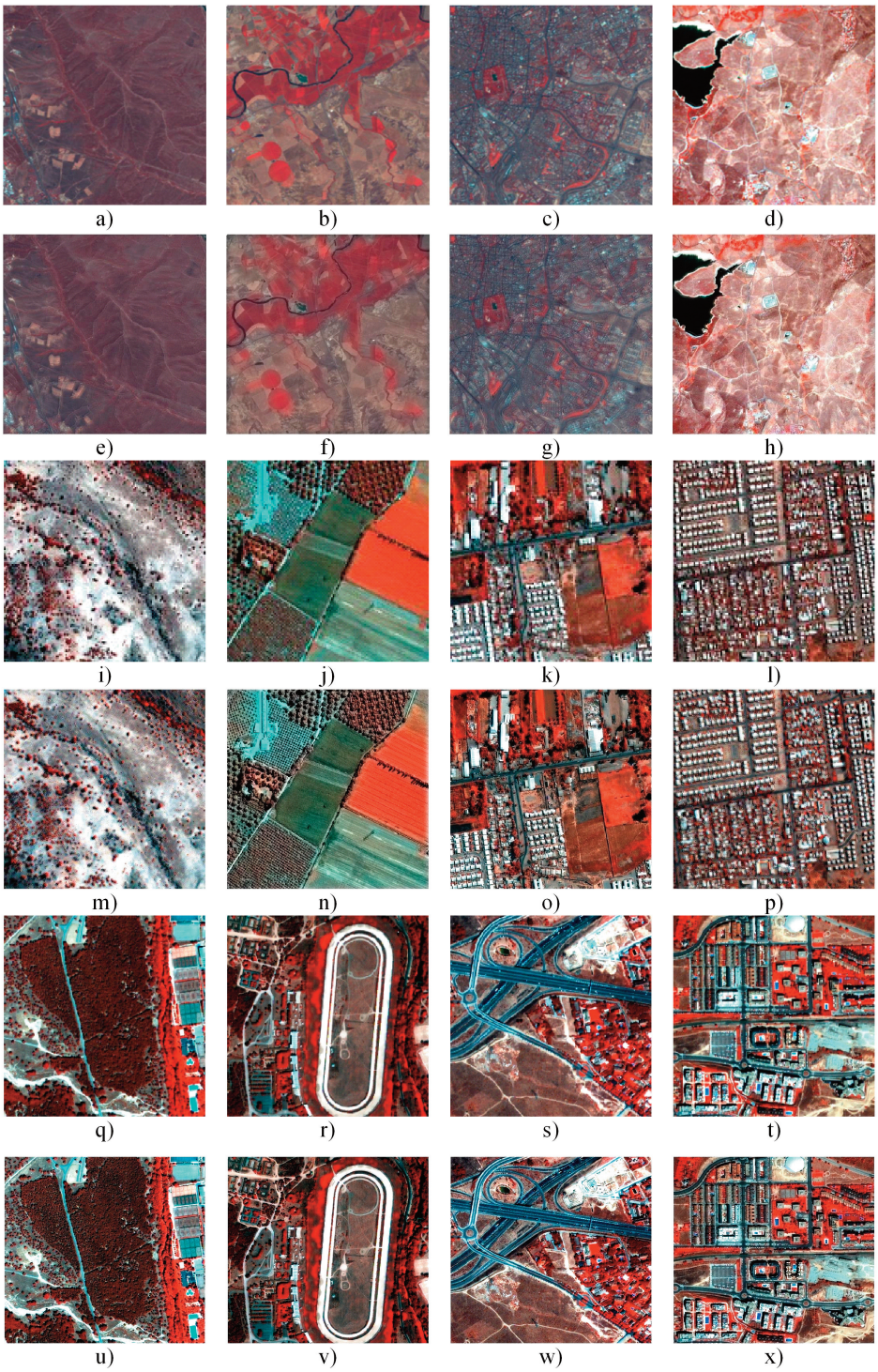

Figure 4. 1st row: NGB compositions of the Landsat MULTI scenes, L1 (a), L2 (b), L3 (c) and L4 (d). 2nd row: NGB compositions of the Landsat fused scenes for n=2 (e), 5 (f), 2 (g), and 2 (h). 3rd row: NGB compositions of the Ikonos MULTI scenes, IK1 (i), IK2 (j), IK3 (k) and IK4 (l). 4th row: NGB compositions of the Ikonos fused scenes for n=1 (m), 4 (n), 1 (o), and 2 (p). 5th row: NGB compositions of the Quickbird MULTI scenes, QU1 (q), QU2 (r), QU3 (s), and QU4 (t). 6th row: NGB compositions of the Quickbird fused scenes for n=3 (u), 3 (v), 3 (w), and 4 (x).

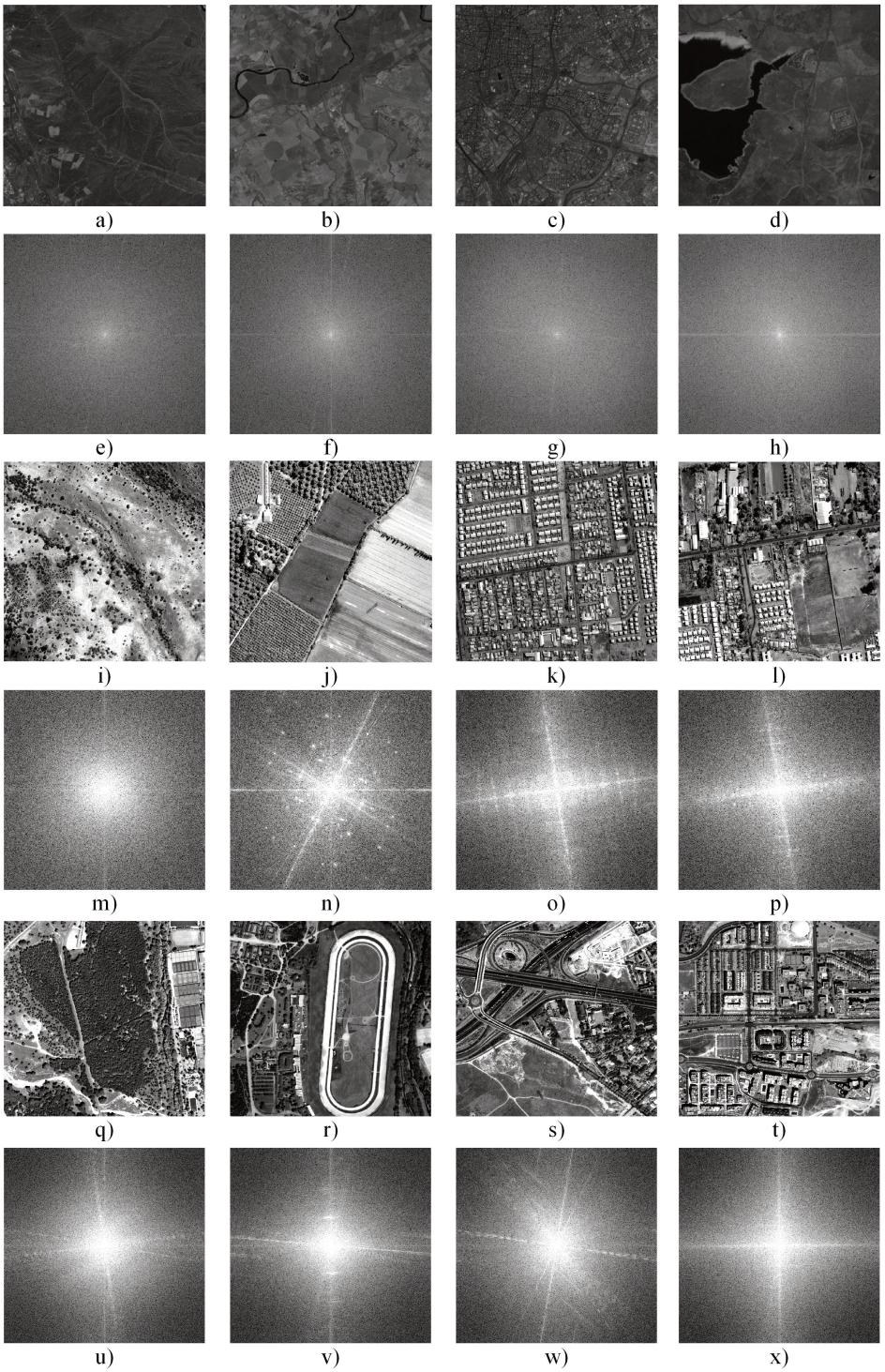

Figure 5. 1st row: Pancromatic Landsat scenes, L1 (a), L2 (b), L3 (c) and L4 (d). 2nd row: FFT modules in logarithmic scale of Pancromatic Landsat scenes, L1 (e), L2 (f) L3 (g) and L4 (h). 3rd row: Pancromatic Ikonos scenes, IK1 (i), IK2 (j), IK3 (k) and IK4 (l). 4th row: FFT modules in logarithmic scale of Pancromatic Ikonos scenes, IK1 (m), IK2 (n) IK3 (o) and IK4 (p). 5th row: Pancromatic Quickbird scenes, QU1 (q), QU2 (r), QU3 (s), and QU4 (t). 6th row: FFT modules in logarithmic scale of Pancromatic Quickbird scenes QU1 (u), QU2 (v), QU3 (w), and QU4 (x).

Scene IK4 (Figures 4 (l) 5 (l)) has an area that contains different coverage types. Its Fourier Transform (Figure 5 (p)) presents some similarities with the one of IK3, but the intensity of high frequencies is much lower.

The Quickbird scene QU1 (Figures 4 (q) and 5 (q)) corresponds principally to a zone of natural tree vegetation. Similar to L1 and IK1 scenes, it can be observed that the FFT (Figure 5 (u)) presents lower intensity in high frequency than the rest of the scenes recorded by the same sensor. The other three scenes correspond fundamentally to urban zones (QU2 (Figures 4 (r) and 5 (r)), QU3 (Figures 4 (s) and 5 (s)), and QU4 (Figures 4 (t) and 5 (t))), although they present notorious differences in coverage type: a large section of QU2 corresponds to playing fields, there is a significant presence of communication paths in QU3, and QU4 corresponds to an urban zone similar to the IK4 scene of the Ikonos images. When the FFT of the scenes are compared (Figures 5 (v) (w) and (x)), it can be observed that QU2 and QU3 present symmetries with different orientations, while QU4 principally has horizontal and vertical regularity. Additionally, QU4 presents a higher intensity of high frequencies in the FFT axis than the other three scenes with the same type of images.

Given the concept of fusion that underlies the algorithm used in this study, it is expected that the differences presented in the distinct scenes from the point of view of spatial frequencies content, have a clear influence on the decomposition level to which the source images have to be submitted. Concretely, it would be reasonable to think that those scenes with greater spatial frequency content would require higher decomposition levels, which would permit integrate a larger quantity of detail coming from the panchromatic images in the different bands of the corresponding multispectral image.

RESULTS

The methodology proposed in Section 3 has been applied to each one of the scenes described in the Section 4, for five values of the decomposition level (n=1, 2,…, 5). ERGAS index values, statistics indicators (average and standard deviation) and their product, as well as, the spectral and spatial correlation indices and the global Q4 index, have been evaluated for each one of the sixty resulting fused images. Tables 1, 2 and 3 for the Landsat, Ikonos and Quickbird scenes, respectively, summarize the indices values.

In Tables 1, 2 and 3, it can be appreciated the similar tendency between the pairs of indices spectral ERGAS and spectral correlation, and spatial ERGAS, and spatial correlation, respectivley.

However, it can be observed that the correlation indices present saturation effects, as it has been mentioned before. While the ERGAS indices present a higher sensitivity to the decomposition level variations.

Results included in Tables 1, 2 and 3 show that the Q4 index has the same quality tendency that the average values of the ERGAS indices: the spatial-spectral quality of the image diminishes as the decomposition level increases. That confirms the global character of the average ERGAS indices.

Moreover it should be pointed the adequate behavior of the quality trade-off indicators proposed in this work (Avxσ), since they decrease as the decomposition level increases until a particular value of n, for which the minimum values is gotten.

For Landsat scenes (Table 1), the decomposition levels that provide the best quality trade-off for the fused images have been, for scenes L1, L3 and L4, n=2, and for scene L2, which presents higher spatial frequencies in its FFT, n=5. It should be noted that for Landsat scenes, the average ERGAS values associated with the best quality trade-off are close to 2 for L1, close to 3 for L3 and L4 and higher than 3 for L2. Therefore it can be concluded that the global quality of the fused scenes L2, L3 and L4 are not good enough, for the values of n that present the best compromise between spatial and spectral quality, as it can be appreciated in Fig. 4 (e), (f), (g) and (h), where images fused from Landsat scenes are included. From the results, it seems that for this kind of images, the decomposition level that provides the best quality trade-off is 2.

Also for Ikonos scenes has been observed that scenes with greater content of high spatial frequencies require higher decomposition levels. Thus, for scenes IK1 and IK3, the minimum product values (Avxσ) have been obtained for n=1, and for IK4 n=2; while, IK2 requires n=5, as it can be expected, given its high content of spatial frequencies. In this last case, it can be observed that the source images would need to be degraded more than 5 times to obtain a fused image with an $ERGAS_{spatial}$ less than 3. However, this assumes that the $ERGAS_{spectral}$ would exceed this threshold. Given that in this case, the criterion of less minimum product (0.2038) provides an average ERGAS index greater than 3, the most adequate decomposition level could be considered

n	ERGAS					SC	I_Z	Q4
	Spectral	Spatial	Aver.(Av)	Dev.(σ)	Av × σ			
				L1				
1	1,1096	2,8184	1,9640	1,2083	2,3731	0,9578	0,9451	0,9629
2	**1,8555**	**2,2084**	**2,0320**	**0,2495**	**0,5070**	**0,8627**	**0,9912**	**0,8731**
3	2,3850	1,8963	2,1407	0,3456	0,7398	0,7917	0,9950	0,8025
4	2,8262	1,7504	2,2883	0,7607	1,7407	0,7480	0,9959	0,7575
5	3,2297	1,6876	2,4587	1,0904	2,6810	0,7175	0,9965	0,7252
				L2				
1	0,9786	4,9475	2,9630	2,8065	8,3156	0,9839	0,9327	0,9892
2	1,7565	4,4941	3,1253	1,9358	6,0500	0,9342	0,9875	0,9525
3	2,3557	4,1682	3,2620	1,2817	4,1807	0,8844	0,9935	0,9130
4	2,8661	3,9297	3,3979	0,7521	2,5556	0,8467	0,9949	0,8808
5	**3,3342**	**3,7394**	**3,5368**	**0,2865**	**1,0133**	**0,8170**	**0,9957**	**0,8537**
				L3				
1	1,7552	4,2324	2,9938	1,7517	5,2442	0,9282	0,9361	0,9335
2	**2,7848**	**3,0538**	**2,9193**	**0,1902**	**0,5552**	**0,7631**	**0,9934**	**0,7731**
3	3,3253	2,4536	2,8894	0,6163	1,7809	0,6491	0,9972	0,6583
4	3,7146	2,1665	2,9405	1,0947	3,2190	0,5883	0,9978	0,5955
5	4,0493	2,0134	3,0314	1,4396	4,3640	0,5518	0,9981	0,5570
				L4				
1	1,7438	3,7658	2,7548	1,4298	3,9388	0,9782	0,9513	0,9782
2	**3,0431**	**2,8117**	**2,9274**	**0,1636**	**0,4789**	**0,9312**	**0,9965**	**0,9313**
3	3,9265	2,3270	3,1268	1,1310	3,5365	0,9030	0,9989	0,9033
4	4,6484	2,0445	3,3464	1,8412	6,1615	0,8887	0,9993	0,8890
5	5,2963	1,8433	3,5698	2,4417	8,7163	0,8802	0,9994	0,8806

Table 1. Fused Landsat images quality indices.

n	ERGAS					SC	I_Z	Q4
	Spectral	Spatial	Aver.(Av)	Dev.(σ)	Av × σ			
				IK1				
1	**0.8904**	**1.0238**	**0.9571**	**0.0943**	**0.0903**	0.9907	0.9447	0.9121
2	1.3513	0.6855	1.0184	0.4708	0.4795	0.9712	0.9477	0.8354
3	1.6392	0.5331	1.0862	0.7821	0.8495	0.9470	0.9457	0.8012
4	1.8368	0.4560	1.1464	0.9764	1.1193	0.9260	0.9455	0.7828
5	1.9883	0.4086	1.1985	1.1170	1.3387	0.9105	0.9461	0.7694
				IK2				
1	1.4868	3.7275	2.6071	1.5844	4.1307	0.9867	0.9445	0.7910
2	2.2417	3.4617	2.8517	0.8626	2.4599	0.9607	0.9501	0.6385
3	2.6189	3.3387	2.9788	0.5090	1.5162	0.9338	0.9492	0.5838
4	2.8836	3.2527	3.0682	0.2610	0.8008	0.9113	0.9494	0.5525
5	**3.0847**	**3.1768**	**3.1308**	**0.0651**	**0.2038**	0.8946	0.9502	0.5295
				IK3				
1	**1.6845**	**1.9666**	**1.8256**	**0.1995**	**0.3642**	0.9339	0.9427	0.8078
2	2.5972	1.2205	1.9089	0.9735	1.8583	0.8718	0.9477	0.6635
3	3.1255	0.8270	1.9762	1.6253	3.2119	0.8412	0.9434	0.6158
4	3.4469	0.6218	2.0343	1.9976	4.0637	0.8222	0.9424	0.5973
5	3.6498	0.5088	2.0793	2.2211	4.6183	0.8087	0.9432	0.5890
				IK4				
1	1.4887	2.2337	1.8612	0.5268	0.5798	0.8922	0.9773	0.9333
2	**2.2603**	**1.8037**	**2.0320**	**0.3229**	**0.0586**	0.7851	0.9922	0.8692
3	2.7448	1.5869	2.1658	0.8188	0.5125	0.7291	0.9934	0.8383
4	3.0963	1.4481	2.2722	1.1655	0.8596	0.6975	0.9940	0.8198
5	3.3592	1.3474	2.3533	1.4225	1.1552	0.6806	0.9945	0.8069

Table 2. Fused Ikonos images quality indices.

n	ERGAS					SC	I_Z	Q4
	Spectral	Spatial	Aver.(Av)	Dev.(σ)	Av × σ			
				QU1				
1	0.9225	2.9270	1.9247	1.4174	1.1315	0.9592	0.9521	0.9854
2	1.7217	2.5570	2.1394	0.5907	0.4729	0.9356	0.9754	0.9560
3	**2.2809**	**2.3205**	**2.3007**	**0.0280**	**0.1771**	0.9196	0.9713	0.9348
4	2.6863	2.1572	2.4217	0.3741	0.8376	0.9086	0.9694	0.9208
5	2.9966	2.0294	2.5130	0.6839	1.5013	0.8999	0.9691	0.9105
				QU2				
1	0.5731	1.8786	1.2258	0.9231	2.7281	0.9722	0.9493	0.9936
2	1.1334	1.6194	1.3764	0.3436	1.2637	0.9603	0.9821	0.9767
3	**1.6047**	**1.4403**	**1.5225**	**0.1163**	**0.0644**	0.9511	0.9830	0.9637
4	2.0224	1.3119	1.6671	0.5024	0.9060	0.9442	0.9830	0.9541
5	2.3914	1.2133	1.8023	0.8330	1.7186	0.9387	0.9833	0.9494
				QU3				
1	0.7741	2.1294	1.4517	0.9583	1.3912	0.9454	0.9569	0.9780
2	1.4159	1.7922	1.6040	0.2661	0.4268	0.9131	0.9871	0.9347
3	**1.8637**	**1.5875**	**1.7256**	**0.1953**	**0.3370**	0.8912	0.9887	0.9030
4	2.1744	1.4629	1.8186	0.5031	0.9149	0.8768	0.9891	0.8833
5	2.3950	1.3758	1.8854	0.7207	1.3588	0.8666	0.9896	0.8787
				QU4				
1	0.6167	2.2568	1.4368	1.1597	1.6663	0.9276	0.9606	0.9748
2	1.1051	1.9849	1.5450	0.6221	0.9611	0.8916	0.9882	0.9310
3	1.4627	1.8289	1.6458	0.2590	0.4263	0.8699	0.9899	0.9027
4	**1.7418**	**1.7375**	**1.7397**	**0.0031**	**0.0054**	0.8553	0.9909	0.8842
5	1.9676	1.6796	1.8236	0.2036	0.3713	0.8433	0.9919	0.8701

Table 3. Fused Quickbird images quality indices.

to be 3, since, even when there is a lower compromise between spatial and spectral quality of the image (deviation = 0.5090), the average ERGAS does not exceed the established threshold.

Based on these results and given the characteristics of the IK4 scene, in which there is no type of dominant coverage, and consequently it can be understood as a representative Ikonos scene, the authors consider that a decomposition level of n=2 is adequate to fuse this type of image, which confirms the experimental results obtained by other authors (Nuñez *et al*. 1999; Wald 2002).

Fig. 4 (m), (n), (o), and (p) represent fused images of the Ikonos scenes for the values of n that provide the best spectral-spatial quality trade-off. In all of them, it can be appreciated a notable spatial quality increase, while maintaining the spectral quality provided by the MULTI image.

The methodology proposed has allowed determining that the Quickbird scenes QU1, QU2, and QU3, which contain different coverage types that correspond to medium frequencies distribution in the Fourier domain, require a decomposition level of n=3. However, QU4, which is characterized by a high content of spatial frequencies, requires 4 decomposition levels. In this last case, it can be observed that a good equilibrium between the spatial and spectral quality of the fused images has been obtained, since the deviation between the two ERGAS indices is reduced to 0.0031. Considering these results, the authors propose the value of n=3 as adequate for the fusion of Quickbird images that do not present high spatial variability.

Fig. 4 (u), (v), (w), and (x) represent images fused from Quickbird scenes for the values of n that present the best compromise between spatial and spectral quality.

CONCLUSIONS

The availability of two very sensitive indices, spatial and spectral ERGAS, that measure spatial and spectral quality of the fused images independently, but within the same domain, without saturation effects, has permitted to research the dependence of the trade-off between the corresponding quality, respect to the decomposition level (n) to which the source images are subjected.

Furthermore, the product of the average value of the ERGAS indices and its standard deviation has shown to be a very good indicator to determine the

decomposition level (n) that provides the best trade-off between spatial and spectral quality of the fused images.

The results obtained in this study, have experimentally demonstrated that the decomposition level that provides fused images with better global quality depends on the spatial characteristics of the source images. It was observed that for images with a high content of spatial frequencies, high decomposition levels are required. However, it should be pointed that in the majority of the cases, a low number of decompositions provides fused images with a high spatial and spectral quality trade-off. Thus, general speaking, a value of n=2 have been obtained for Landsat scenes, n=2 seems to be adequate for Ikonos scenes and n=3 for Quickbird images.

ACKNOWLEDGMENTS

This work has been jointly supported by the Technical University of Madrid, Spain (AL08-P(I+D)-19), the Spanish Government (TEC2007-60607/TCM) and Chile Research Council (FONDECYT 11060056). The authors would like to thank the company INDRA-Espacio for facilitating the Quickbird image used in this study.

REFERENCES

ALPARONE L., S. Baronti, A. Garzelli, F. Nencini, , 2004, A global quality measurement of pan-sharpened multispectral imagery. *Geosci. Rem. Sens. Lett. IEEE* 1 (4), 313-317. [doi:10.1109/LGRS.2004.836784].

CANDES E. J., and D. L. Donoho, 2000, Curvelets, Multiresolution Representation, and Scaling Laws. In *Wavelet Applications in Signal and Image Processing VIII, Proc. SPIE* 4119, 1-12. [doi:10.1117/12.408568].

CHIBANI Y., and A. Houacine, "Redundant versus orthogonal Wavelet decomposition for multisensor image fusion", *Pattern Recogn.* 36, 879-887 (2003) [doi:10.1016/S0031-3203(02)00103-6].

DUTILLEUX P., 1987, An implementation of the algorithm à trous to compute the wavelet transform. In: *Compt-rendus du congrès ondelettes et méthodes temps-frequence et espace des phases*, Springer-Verlag, Marseille, 298-304.

GONZÁLEZ-AUDICANA M. , X. Otazu, O. Fors, and A. Seco, 2005, Comparison between the Mallat' s and the à trous discrete wavelet transform based algorithms for the fusion of multispectral and panchromatic images. *Int. J. Rem. Sens.* 26, 597-616. [doi: 10.1080/01431160512331314056].

GONZALO C., and M. Lillo-Saavedra, 2004, Customized fusion of satellite images based on a new à trous algorithm. *In Image and Signal Processing for Remote Sensing X, Proc. SPIE* 5573, 444-451. [doi:10.1117/12.565216].

LILLO-SAAVEDRA M. and C. Gonzalo, A. Arquero, and E. Martinez, 2005. Fusion of multispectral and panchromatic satellite sensor imagery based on tailored filtering in the Fourier domain. *Int. J. Rem. Sens*. 26, 1263-1268. [doi:10.1080/01431160412331330239].

LILLO-SAAVEDRA M. and C. Gonzalo, 2006. Spectral or spatial quality for fused satellite imagery? A trade-off solution using wavelet à trous algorithm. *Int. J. Rem. Sens.* vol.27, 7:1453-1464.[doi:10.1080/01431160500462188]

MALFAIT M., and D. Roose, 1997, Wavelet-based image denoising using a Markov random field a priori model. *IEEE Trans. Image Process.* 6, 549–565. [doi:10.1109/83.563320].

MALLAT S., 1999, *A Wavelet Tour of Signal Processing,* 2nd ed., Academic Press, London.

MATHER P. M, 1999, *Computer of Remotely Sensed Images; An Introduction*, 2nd Ed., Wiley.

NÚÑEZ J., X. Otazu, O. Fors, A. Prades, V. Palá, and R. Arbiol, 1999, Multiresolution-based image fusion with additive wavelet decomposition. *IEEE Trans. Geosci. Rem. Sens.* 37, 1204-1211. [doi:10.1109/36.763274].

PIELLA G., and H. Heijmans, 2003, A new quality metric for image fusion. In: *Proceedings International Conference on Image Processing,* 3, 173-176. [doi: 10.1109/ICIP.2003.1247209].

POHL A., 1997, Tools and methods for fusion of images of different spatial resolution. *Int. Arch. Photogramm. Rem. Sens.* 32, 7-11.

POHL C., and J. L.van Genderen, 1998 ,Multisensor image fusion in remote sensing: concepts, methods and application. *Int. J. Rem. Sens.* 19, 823-854. [doi:10.1080/014311698215748].

QU G. H., D. L. Zhang, and P. F. Yan, 2002, Information measure for performance of image fusion. *Electron. Lett*. 38 (7), 313–315. [doi: 10.1049/el:20020212].

RANCHIN T., B. Aiazzi , L. Alparone, S. Baronti, and L. Wald, 2003, Image fusion -the ARSIS

concept and some successful implementation schemes. *ISPRS J. Photogramm. Rem. Sens*. 58, 4-18. [doi:10.1016/S0924-2716(03)00013-3].

SAWAYA K., L. Olmanson, N. Heinert, P. Brezonik, and M. Bauer, 2003, Extending satellite remote sensing to local scales: land and water resource monitoring using high-resolution imagery. *Rem. Sens.* Environ. 88, 144-156 [doi:10.1016/j.rse.2003.04.006].

UNSER M., 1995, Texture classification and segmentation using wavelet frames. *IEEE Trans. Image Process.* 4, 1549–1560. [doi:10.1109/83.469936].

WALD L., 2002, *Data Fusion, Definition and Architectures: Fusion of Image of Different Spatial Resolution,* Le Presses de l'École des Mines, Paris.

WANG Z., and A. C. Bovik, 2002, A universal image quality index. *IEEE Signal Process. Lett.* 9 (3), 81-84 [doi: 10.1109/97.995823].

XYDEAS C., and V. Petrovi´c, 2000, Objective pixel-level image fusion performance measure. *In Sensor Fusion: Architectures, Algorithms and Applications IV, Proc. SPIE* 4051, 88–99. [doi:10.1117/12.381668].

ZHANG Y., and G. Hong, 2005, An IHS and wavelet integrated approach to improve pan-sharpening visual quality of natural colour Ikonos and QuickBird images. *Inform. Fusion* 6, 225–234. [doi:10.1016/j.inffus.2004.06.009].

ZHOU J., D. L. Civco, and J. A. Silander, 1998, A wavelet transform method to merge Landsat TM and SPOT panchromatic data". *Int. J. Rem. Sens.* 19 (4), 743–757. [doi:10.1080/014311698215973].